

Combining SVD and Co-occurrence Matrix Information to Recognize Organic Solar Cells Defects with a Elliptical Basis Function Network Classifier

Grazia Lo Sciuto¹, Giacomo Capizzi¹, Dor Gotleyb², Sivan Linde², Rafi Shikler², Marcin Woźniak³(✉), and Dawid Polap³

¹ Department of Electric, Electronic and Informatics Engineering,
University of Catania, Catania, Italy

glosciuto@dii.unict.it, gcapizzi@diees.unict.it

² Department of Electrical and Computer Engineering,
Ben-Gurion University of the Negev, Beersheba, Israel
rshikler@bgu.ac.il

³ Institute of Mathematics, Silesian University of Technology,
Kaszubska 23, 44-100 Gliwice, Poland
{Marcin.Wozniak,Dawid.Polap}@polsl.pl

Abstract. This paper presents a new methodology based on elliptical basis function (EBF) networks and an innovative feature extraction technique which makes use of the co-occurrence matrices and the SVD decomposition in order to recognize organic solar cells defects. The experimental results show that our algorithm achieves an high accuracy of recognition of 96% and that the feature extraction technique proposed is very effective in the pattern recognition problems that involving the texture's analysis. The proposed methodology can be used as a tool to optimize the fabrication process of the organic solar cells. All the tests carried out for this work were made by using the organic solar cells realized in the Optoelectronic Organic Semiconductor Devices Laboratory at Ben Gurion University of the Negev.

Keywords: Organic solar cells · EBFs neural networks · Co-occurrence matrix · Singular Value Decomposition

1 Introduction

The study of organic solar cells (OSCs) has been rapidly developed in recent years. Organic solar cell technology is sought after mainly due to the ease of manufacture and their exclusive properties such as mechanical flexibility, light-weight, and transparency [1]. These properties enable OSCs to be used in unconventional applications which are not suited for conventional solar cells. Nowadays the power conversion efficiencies of OSCs are higher than 10% [2].

This relatively high efficiency and rather low manufacturing costs allows OSCs to be used as an appropriate alternative to other power sources. Nevertheless, currently OSCs are yet to be applicable. In order to extract their full potential OSCs must be optimized. By using the power of computational calculation it can be a relatively simple task to examine, compare, and correlate between both theoretical parameters and physical properties of such device to its performance. According to how the final outcome, i.e., the output power of the device, is affected by its characteristics, e.g., electronic properties, geometry, one can adjust these characteristics to enhance the device performance. It is not yet clear what is the role of defects in the performance of organic solar cells [3]. Therefore, it is critical to examine the correlation between defects in the structure of the device and its performance. Defects can be caused by a variety of reasons, many of them are embedded within the organic materials and physics that governs those kind of devices. However, many of the defects can arise during the OSC fabrication stage. These defects can emerge for example by scratches that occurs during different stages of fabrication, or by trapped microscopic bubbles during the spin coating stage. Thus, identification and inspection of defects can lead to the improvement and preciseness in fabrication and to a more informed decision of the materials that should be used. By taking microscopic images of the morphology of the OSC and by using a state of the art mathematical models for defects detection we were able to detect, identify, and classify these defects. In most common approaches we can discuss various types of information analysis where initial data is processed by application of some fuzzy measures [5] or image processing for extraction of most important features [4, 6–8]. In this paper we would like to discuss a novel methodology based on neural network classifier.

2 Materials

Solar cells are devices that convert sunlight into electrical power. The process of light conversion takes place in the organic layer, which will be referred as the active layer. This active layer is a composition of two organic materials (blend). These two materials are similar to the semiconductors used in the inorganic industry. Just like in semiconductors, organic materials possess a band-gap between two bands, namely, the Highest Occupied Molecular Orbital (HOMO) band and the Lowest Unoccupied Molecular Orbital (LUMO) band; the occupation refers to the organic molecule electrons. The HOMO and LUMO of organic materials are analogous to the conduction and valence bands in the inorganic semiconductors respectively. Typically, the gap between HOMO and LUMO is in the range of 1 to 3eV and thus electrons can be excited, for instance, by light in the visible spectrum. Hence, it makes organic semiconductors appropriate for solar cells. Another similarity refer to the materials type. Organic materials are divided into two categories, electron donors and electron acceptors, which are analogues to the n-type (donors) and p-type (acceptors) materials that comprise the corresponding inorganic solar cells counterparts. Donors are hole transport materials and acceptors are electron transport materials, i.e., each exhibits higher mobility for its respective charge carrier.

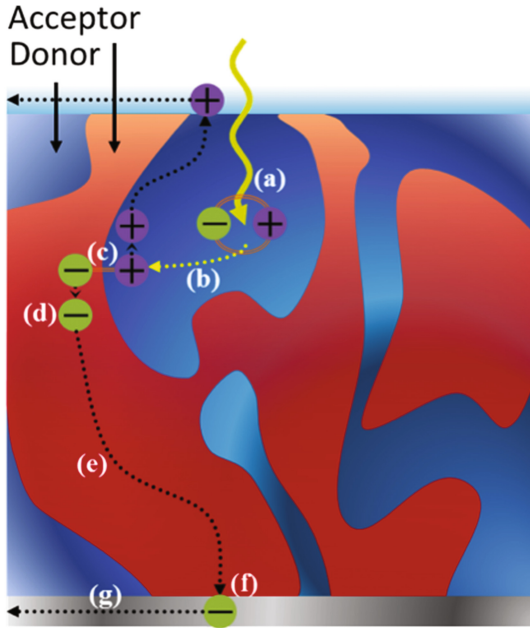


Fig. 1. The processes leading to photocurrent in the bulk heterojunction solar cell. (1) light absorption at the donor lead to the generation of excitons, (2) exciton diffuse towards donor-acceptor interface, (3) an intermediate step where exciton dissociate into $P - P$ state, (4) dissociation of $P - P$ into free two charged polarons, (5) charge transport towards the electrodes, (6) charge collection by the electrodes and charge transport within the electrodes.

The main difference between the organic and inorganic solar cells is the low dielectric constant of the former. As a result, the energy of light (photon energy) is not suffice to separate the electrons and holes into free charges (the charge carriers in a semiconductor). The physical process leading to the generation of current [9] is illustrated schematically in Fig. 1. It is a sequence of the following steps:

1. Light absorption leads to generation of excitons.
2. Exciton diffusion towards donor-acceptor interface.
3. An intermediate step where excitons dissociate into Polaron-Pair ($P - P$) state.
4. Dissociation of $P - P$ into positive and negative polarons.
5. Charge transport towards the electrodes.
6. Charge collection by the electrodes.

As sunlight absorbs in a molecule, an electron is excited from the LUMO to the HOMO. The absorption occurs mostly in the donor material. However, instead of free charges, an exciton is generated, an electron and hole bounded

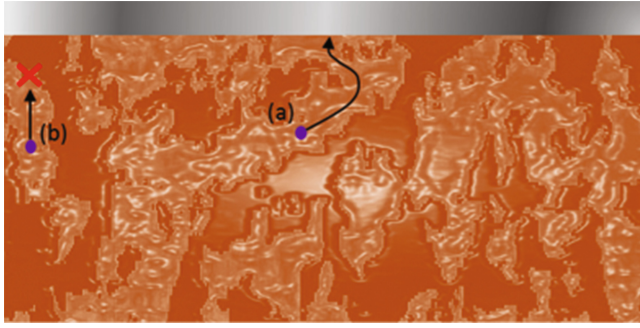


Fig. 2. An illustration of the morphology. The top gray strip stands for the ITO, the bright and dark orange signifies the acceptor and donor respectively, the purple points are the electrons and the arrows represents the path of the electrons to the ITO. (a) A path for the negatively charged polaron. (b) there is no direct path for the polaron. (Color figure online)

together by coulomb force within a molecule. It is a direct outcome of the low dielectric constant. In order to separate the exciton into free charges, the exciton must diffuse and encounter an interface between donor and acceptor materials (heterojunction). The excitons have a very low diffusion length, in the order of 10 nm. Above this length, the excitons will recombine and will not contribute to the output current. With the appropriate combination of donor and acceptor, the exciton can lower his energy by transferring one of the charges to the adjacent material. If exciton was initially created at the donor (acceptor), then electron (hole) will transfer to the acceptor (donor), namely, electron is situated at the acceptor and hole at the donor. Yet, the electron and hole are still coulomb bound. This intermediate state between excitons and free charges is the Polaron-Pair ($P - P$). Depending on the electric field, the temperature, and the materials parameters there is a finite probability for the $P - P$ to decay to the ground state or to be separated into two charged polarons (electron and hole), i.e., $P - P$ dissociation. This non-zero probability ensures the generation of free polarons. After the separation, the free polarons must diffuse and be collected at the corresponding contacts. Negatively charged polarons move in the acceptor material and are collected at the cathode and positively charged polarons move in the donor and are collected at the anode.

As was mentioned before, the active layer is made of a blend of both the donor and acceptor materials composed in a single layer. In this fashion, junctions between donors and acceptors are spatially distributed throughout the active layer. Hence, this type of OSC often called bulk heterojunction (BHJ). The obtained phase separation (separation between donor and acceptor materials) within the film is less than 30 nm [10] which is in the range of the exciton diffusion length. Thus, regardless of where an exciton generates, it will most likely encounter a junction. This formation enhances the exciton dissociation within the active layer. However, defects in the structure of the active layer can drastically reduce the output power. By inspecting the microscopic images of the

active layer, one can examine whether the morphology is satisfactory or whether it needs further optimizations.

Yet another very important issue is the transportation of free polarons from the position of the specific junction to the respective contact. The downside of this blend morphology is the large extent of disorder. In the path to the desired contact, the free polarons can stumble upon different interface and recombine again to $P - P$. Although it can lead again to the dissociation of $P - P$ to free polarons, it interferes their movement and increases the chance to decay to the ground state. Therefore, knowing how the different materials and fabrication processes affects the final morphology is crucial for the process of improvement. This can be achieved by examining microscopic images and examine them by means of computational models. An illustration of the morphology is shown in Fig. 2. Once again, using such images one can detect defects that can impair the path of free carriers to the electrodes.

3 Architecture of OSC

The OSC built up as an assemblage of several layers of different materials and different functionalities. A typical cross-section of an OSC is shown in Fig. 3. It composed of the following layers, in the direction of the incoming light, transparent substrate, transparent anode, active layer, and cathode.

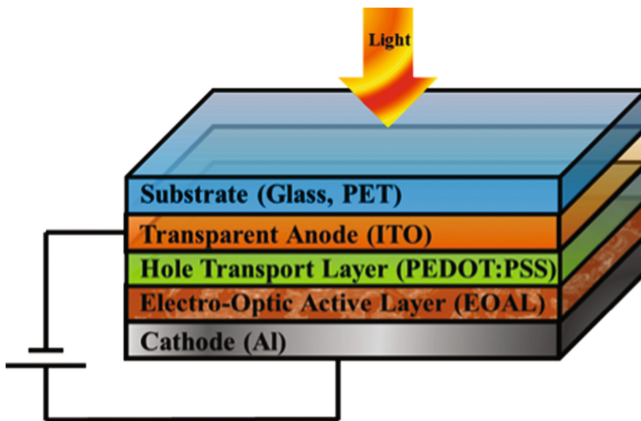


Fig. 3. A typical cross section of an organic solar cell. From the direction of the incoming light, transparent substrate (glass), transparent anode (ITO), Hole Transport Layer (PEDOT:PSS) optoelectronic active layer (P3HT:PCBM) and cathode (Aluminum).

The fabrication and measurements of the OSCs took place in the “Optoelectronic Organic Semiconductor Device Laboratory” (OOSDL) in the department of Electrical and Computer Engineering at Ben-Gurion University of the Negev

in Beer-Sheva, Israel. In order to create large database, a series of samples has been made, where each sample comprised of four solar cells.

The substrate of the sample is a glass with a thickness of 0.7 mm coated with a 90 ± 10 nm layer of Indium Tin Oxide (ITO), i.e., the transparent anode. The area of the substrate is 12×12 mm². The ITO covers only 6×12 mm² of the glass and has a resistivity of 20 Ω /m². The active layer of the sample is a solution blend of [6, 6]-Phenyl C61 Butyric acid Methyl ester (PCBM) and Poly(3-Hexylthiophene-2, 5-diyl) (P3HT) with 1:1 ratio. The solution is dissolved in chloroform with the aid of a magnetic stirrer for one hour to make a total of 20 mg/ml. The preparation is a sequence of few procedures. First, the substrate was cleaned in an ultrasonic bath with acetone, then methanol and then isopropanol for 15 min each; next, it was treated with UV-ozone for 4 min. To facilitate the conduction of holes from the active layer to the ITO we spin coated on top of the glass+ITO a 30 nm layer of a transparent and conducting conjugated polymer Poly(3, 4-ethylenedioxythiophene)-poly(styrenesulfonate) (PEDOT:PSS). The spin coating was performed at 5000 RPM, and 1700 acceleration for 1 min. Afterwards, the sample was dried on a hot plate at 105° C for an half an hour to remove the excess water, and then for another half an hour inside a glove-box. Inside this inert atmosphere, the solution of P3HT:PCBM was then deposited by spin-casting (1000 RPM, and 600 acceleration for 1 min) at room temperature. At the top of the sample, the contact pattern was thermally evaporated to create 80 nm thickness layer of aluminum, i.e., the cathode. The sample was then annealed at 140°C for 20 min. To expose the ITO, we screeched the active layer with a toothpick. Finally, to make the contacts accessible for the external probes, we deposited on top of ITO and aluminum a conductive silver epoxy. A typical OPV sample realized is shown in Fig. 4.

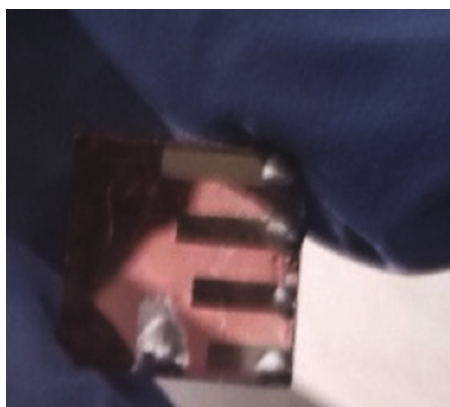


Fig. 4. A typical OPV sample realized at the “Optoelectronic Organic Semiconductor Device Laboratory”.

4 Experimental Image's Dataset and Acquisition System

The images acquisition is performed with a microscope camera DeltaPix, model *DpxViewPro 1.14.8* (see Fig. 5).



Fig. 5. The microscope used to explore the fabrication defects of the organic solar cells.

Microscopy was used to observe the various defects the surface morphology on top of organic solar cells examined. We have acquired 240 images with resolution of 1280×1024 . Some devices analyzed are good, others with various kind of defects.

A large number of defects have been observed which cracks, breaks and scratches. Scratches are caused by mechanical damage or fabrication during the handling and preparation while the shiny spots and the bubbles are due to the water infiltration and at the exposition to the air at high humidity. In addition the annealing process is responsible of the evident spots and the bubbles on surface of samples caused by different gradient temperatures.

A critical aspect is to determine properly on the ITO/aluminum interface the number and type of faults in order to understand the degradation mechanisms providing better encapsulation strategies.

In Fig. 6 we can identify different scratches due to fabrication process at the interfaces of OPV devices.

5 The Feature Extraction Methodology Based on Gray Level Co-occurrence Matrices and Singular Value Decomposition

The degradation mechanisms of the active inter-layers are fast involving the diffusion of molecular oxygen and water into the device inducing chemical reactions in polymer materials, degradation of interfaces, electrode reaction with the

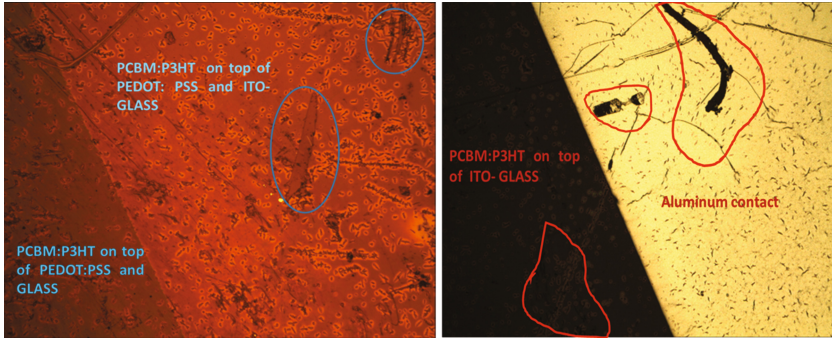


Fig. 6. Defects at the interface PSS and ITO-Glass/PSS and Glass (left), Defects at the interface area on interface PCBM:P3HT on top of ITO-Glass/Aluminum (right).

organic materials, morphological changes due to temperature, and macroscopic changes such as delamination, formation of particles, bubbles, and cracks [11].

The PEDOT:PSS is vulnerable to thermal degradation and also very sensitive to moisture and oxygen involving the irreversible structural modifications. These modifications give rise to a number of defects in the OPVs such as breaks, scratches, spot, bubbles on surface of the device etc. In the SEM images of the OPVs used in this paper, these defects manifest themselves as variation of the image texture.

One of the most popular and powerful ways to describe texture is using of color mapping co-occurrence matrix (GLCM). Since the use of the co-occurrence matrices leads to a course of dimensionality we used the singular value decomposition (SVD) to reduce the redundancy arising of description of the texture by means of the GLCM.

When a high dimensional, highly variable set of data points is taken, SVD is employed to reduce it to a lower dimensional space that exposes the substructure of the original data more clearly and orders it from most variation to the least. In this way, the region of most variation can be found and its dimensions can be reduced using the method of SVD. This implies that we can achieve a good identification of the most significant structures present in the image texture, by taking only a few largest singular values [12].

Color Mapping Co-occurrence Matrix. A GLCM is a square matrix where the number of rows and columns is equal to the number of gray levels in the image that can reveal certain properties about the spatial distribution of the gray-levels in the image texture [13, 14]. The matrix gives how the pixel value l_1 of a reference pixel occurs in a specific relationship to a neighbouring pixel with pixel value l_2 . So, each element (l_1, l_2) of the matrix represents the number of occurrences of the pair of pixel with pixel values l_1 and l_2 which are at a relative distance d from each other. There are many ways to specify the spatial

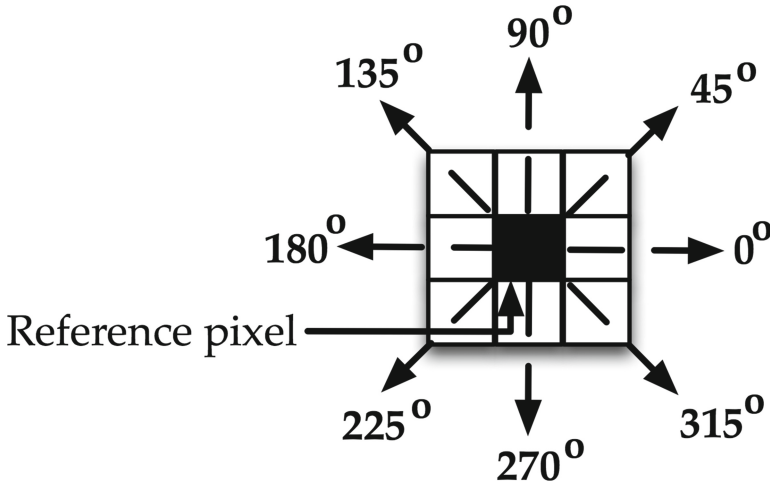


Fig. 7. Co-occurrence matrix directions for extracting texture features.

relationship between two neighbouring pixels with different offsets and angles (see Fig. 7).

Mathematically, the elements of a $L \times L$ gray-level co-occurrence matrix with displacement vector $\mathbf{d}(= d_i, d_j)$, for a given image I of size $n \times n$ is defined as:

$$M_{CO}(l_1, l_2) = \sum_{i=1}^n \sum_{i=1}^n \begin{cases} 1, & \text{if } I(i, j) = l_1 \text{ and } I(i + d_i, j + d_j) = l_2 \\ 0, & \text{otherwise} \end{cases} \quad (1)$$

Figure 7 describes how to compute the GLCM. It shows an image and its corresponding co-occurrence matrix using the default pixels spatial relationship (offset = +1 in i direction). Each element of the GLCM is the number of times that two pixels with gray tone l_1 and l_2 are in neighborhood at a distance d and direction ϕ .

Singular Value Decomposition. SVD is a potent mathematical exploration tool for matrices which gives minimum least square truncation error [15, 16]. This is because the total potential degrees of freedom of the decomposed matrices is equal to the input host image. Further, SVD is a single path decomposition algorithm. Singular values represent inherent algebraic image properties and are not instable. Given an image $I(x, y)$, with dimensions $m \times n$, it can be factorized with SVD:

$$I = USV^T \quad (2)$$

Where both U and V are the orthonormal matrices, $U \in R^{m \times m}$, $V \in R^{n \times n}$, $S = [diag(\sigma_1, \sigma_2, \dots, \sigma_q), 0]$ and $q = \min(m, n)$. Besides, the singular values appear in descending order, i.e., $\sigma_1 \geq \sigma_2 \geq \dots \geq \sigma_q \geq 0$.

The Feature Extraction. The training set must be thoroughly representative of the actual population for effective classification. We have calculated the co-occurrence matrices of every image. For each channel (Red, green, Blue) we have calculated the co-occurrence matrices for $d = 1, 2$ and in the four main directions: 0° , 45° , 90° and 135° .

The use of the co-occurrence matrices leads to a course of dimensionality because these matrices are composed of two complementary subspaces called signal subspace (the information suitable for defects classification) and noise subspace. To achieve the separation between signal and noise we have been using the SVD and for each co-occurrence matrix we took the 12 largest singular values (the criterium of truncation is $\frac{\sigma_i}{\sigma_{i+1}} \geq 10$), thus obtaining for each image a feature vector of 216 elements.

The magnitude of the singular values indicate the importance of the corresponding directions (vectors). The singular values reflect the amount of data variance captured by the basis elements. The first vector of the basis (the one with largest singular value) lies in the direction of the greatest data variance. The second vector captures the orthogonal direction with the second greatest variance, and so on.

This is a useful procedure because the entries of co-occurrence matrices have a large variance in correspondence of an irregular texture while a lower variance when the texture is regular.

The Figs. 8 and 9 show a marked difference between features belonging to the defective devices and the good ones. Then this feature set proves extremely suitable for the problem classification addressed in this paper.

6 The Used EBF Classifier

A PNN is predominantly a classifier: Map any input pattern to a number of classifications (in our case the neural network has to distinguish between two classes: the defective devices and the good ones). A PNN is an implementation of a statistical algorithm called kernel discriminant analysis in which the operations are organized into a multilayered feedforward network with four layers:

- Input layer
- Pattern layer
- Summation layer
- Output layer

In this paper we make use of a particular kind of PNN: the EBF network [17] that is a type of feedforward neural networks in which the hidden units evaluate the distance between the input vectors and a set of vectors called function centers or kernel centers (the centers are the data points of the training set), and the outputs are a linear combination of the hidden nodes' outputs. More specifically, the k -th network output has the form

$$y_k(x(t)) = \sum_{j=1}^M w_{k,j} \Phi_j(x(t)) \quad (3)$$

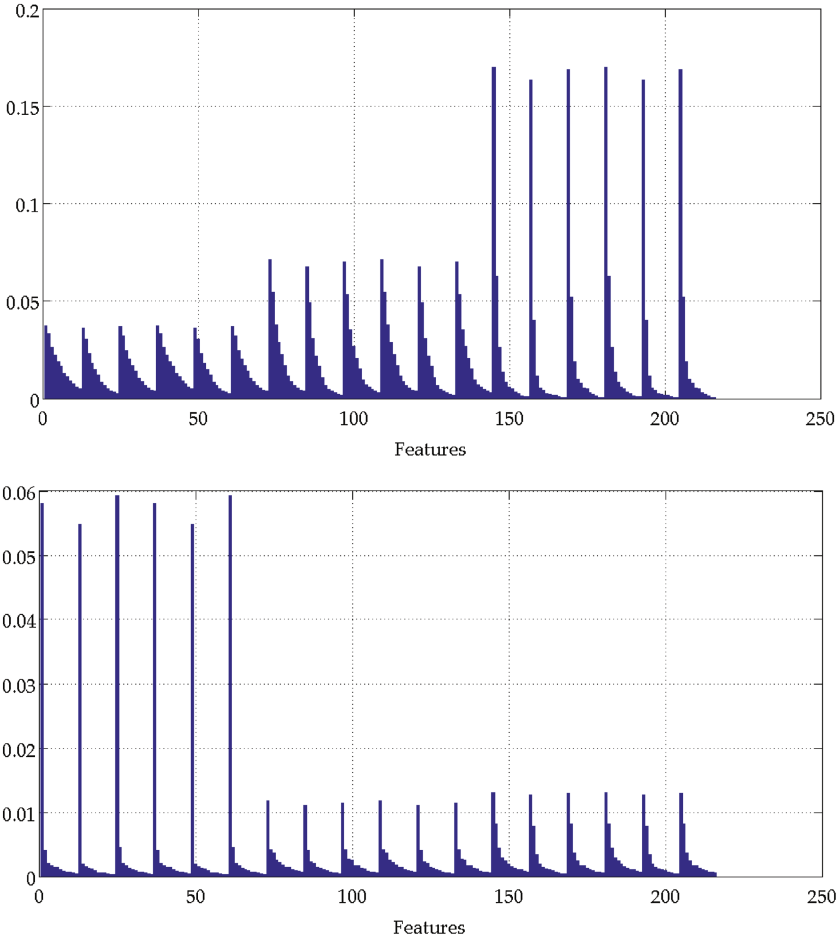


Fig. 8. Features of a defective device randomly chosen (up), Features of a device with no defect randomly chosen (down).

where

$$\Phi_j(x(t)) = \exp \left\{ -\frac{1}{2\sigma_j} (x(t) - \mu_j)^T \Sigma_j^{-1} (x(t) - \mu_j) \right\} \quad (4)$$

μ_j and Σ_j are the function center (mean vector) and covariance matrix of the j -th basis function respectively and σ_j is a smoothing parameter controlling the spread of the j -th basis function.

We restricts Σ to two global and scalar smoothing parameter, σ_1 and σ_2 , where σ_1 is used in those basis functions that have centers coming from the good devices while σ_2 for the defective ones. The determination of the smoothing parameters is done by calculating the spreads of the training data set belonging to the reference classes for σ_1 and σ_2 respectively.

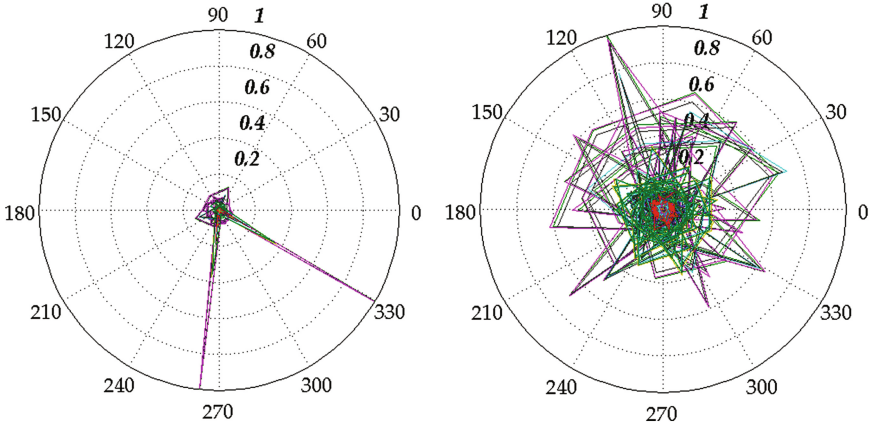


Fig. 9. Features of all defective devices present in the dataset in polar representation (left), Features of all devices with no defect present in the dataset in polar representation (right).

With these assumptions we have that the input nodes (see Fig. 10) are the samples of the feature set. The second layer (pattern layer) consists of the Gaussian functions (5) formed using the training set of data points as centers.

$$y = e^{-\frac{\|x - x_{i,j}\|^2}{\sigma^2}} \tag{5}$$

The third layer (summation layer) performs an weighted average of the outputs from the second layer for each class. The fourth layer (output layer) performs a vote, selecting the largest value (the target values are: 0 for the defective devices and 1 for the good ones).

Adding and removing training samples simply involves adding or removing neurons in the pattern layer and a minimal retraining required.

For the training of the neural network simply note that the centers and spreads are predetermined then only the weights w_{ij} is required to find. The calculation can be performed by using the method of least squares.

The difference between PNN and EBF is that for EBF networks, discrimination among all the known classes is considered during the training phrase; whereas for PNNs this class discrimination is introduced during the recognition phase.

7 Results and Discussion

To evaluate the pattern recognition algorithm, dataset is randomly split into three parts: a training set consisting of 80 data points (48 data points representative of the various kind of defects and 32 representative of the devices with no defects) a validation set consisting of 80 data points and a testing set consisting

of 80 data points. The training set is used to find the model parameters in the used EBF network. These parameters are the number of neuron for each class (the defective devices and the good ones) and the weights value.

To find the optimal number of neurons we proceed as follows:

1. We use the data points of the training set as the centres of the network's neurons, so obtaining a network with 80 neurons split up into two classes (48 neurons represent the defects and 32 represent the devices with no defects).
2. We calculate the network's weights by using the validation set.
3. We eliminate the neuron with a minimum weight and recalculate the network's weights by using the validation set. The procedure ends when the performance, in terms of correct classification on the validation set, falls down of the 2% with respect to the previous step.

The resulting network after the training phase is shown in Fig. 10). It consists of 21 neurons (13 of them represent the defects and 8 represent the devices with no defects).

Once the optimal parameters are found the trained algorithm is applied to classify the data points in the testing dataset into one of the two classes. A correct classification rate of 96% average has been obtained.

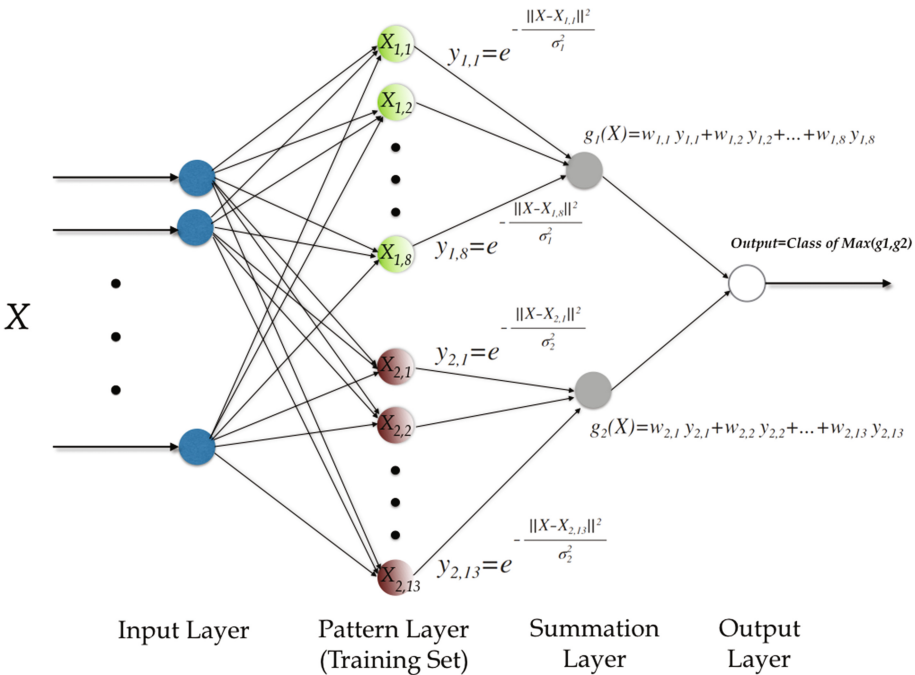


Fig. 10. Architecture of the proposed PNN classifier.

8 Conclusion

This paper presents a new methodology based on elliptical basis function (EBF) networks and an innovative feature extraction technique which makes use of the co-occurrence matrices and the SVD decomposition in order to recognize organic solar cells defects.

The organic solar cells used in this paper were realized in the Optoelectronic Organic Semiconductor Devices Laboratory at Ben Gurion University of the Negev. Microscopy was used to observe the various defects the surface morphology on top of organic solar cells examined. We have acquired 240 images with resolution of 1280×1024 .

A large number of defects have been observed which cracks, breaks and scratches. Scratches are caused by mechanical damage or fabrication during the handling and preparation while the shiny spots and the bubbles are due to the water infiltration and at the exposition to the air at high humidity.

The experimental results show that our algorithm achieves an high accuracy of recognition of 96% and that the feature extraction technique proposed is very effective in the pattern recognition problems that involving the texture's analysis.

The proposed methodology can be used as a tool to optimize the fabrication process of the organic solar cells.

Acknowledgments. Authors acknowledge contribution to this project from the “Diamond Grant 2016” No. 0080/DIA/2016/45 funded by the Polish Ministry of Science and Higher Education.

References

1. Brabec, C.J., Dyakonov, V., Parisi, J., Sariciftci, N.S.: Organic Photovoltaics: Concepts and Realization, vol. 60. Springer Science & Business Media, Berlin (2013)
2. Kan, B., Zhang, Q., Li, M., Wan, X., Ni, W., Long, G., Wang, Y., Yang, X., Feng, H., Chen, Y.: Solution-processed organic solar cells based on dialkylthiol-substituted benzodithiophene unit with efficiency near 10%. *J. Am. Chem. Soc.* **136**(44), 15529–15532 (2014)
3. Gagorik, A.G., Mohin, J.W., Kowalewski, T., Hutchison, G.R.: Effects of delocalized charge carriers in organic solar cells: predicting nanoscale device performance from morphology. *Adv. Funct. Mater.* **25**(13), 1996–2003 (2015). <http://dx.doi.org/10.1002/adfm.201402332>
4. Korytkowski, M., Rutkowski, L., Scherer, R.: Fast image classification by boosting fuzzy classifiers. *Inf. Sci.* **327**, 175–182 (2016). doi:[10.1016/j.ins.2015.08.030](https://doi.org/10.1016/j.ins.2015.08.030)
5. Starczewski, J.T.: Centroid of triangular and gaussian type-2 fuzzy sets. *Inf. Sci.* **280**, 289–306 (2014). doi:[10.1016/j.ins.2014.05.004](https://doi.org/10.1016/j.ins.2014.05.004)
6. Cpalka, K., Zalasinski, M., Rutkowski, L.: A new algorithm for identity verification based on the analysis of a handwritten dynamic signature. *Appl. Soft Comput.* **43**, 47–56 (2016). doi:[10.1016/j.asoc.2016.02.017](https://doi.org/10.1016/j.asoc.2016.02.017)

7. Grycuk, R., Gabryel, M., Nowicki, R., Scherer, R.: Content-based image retrieval optimization by differential evolution. In: IEEE Congress on Evolutionary Computation, CEC, Vancouver, BC, Canada, July 24–29 2016, pp. 86–93. IEEE (2016). doi:[10.1109/CEC.2016.7743782](https://doi.org/10.1109/CEC.2016.7743782)
8. Pabiasz, S., Starczewski, J.T., Marvuglia, A.: SOM vs FCM vs PCA in 3D face recognition. In: Rutkowski, L., Korytkowski, M., Scherer, R., Tadeusiewicz, R., Zadeh, L.A., Zurada, J.M. (eds.) ICAISC 2015. LNCS, vol. 9120, pp. 120–129. Springer, Cham (2015). doi:[10.1007/978-3-319-19369-4_12](https://doi.org/10.1007/978-3-319-19369-4_12)
9. Scarongella, M., Brauer, J.C., Douglas, J.D., Fréchet, J.M.J., Banerji, N.: Charge generation in organic solar cell materials studied by terahertz spectroscopy, pp. 95 670M–95 670M–13 (2015)
10. Heeger, A.J.: 25th anniversary article: bulk heterojunction solar cells: understanding the mechanism of operation. *Adv. Mater.* **26**(1), 10–28 (2014)
11. Balderrama, V.S., Estrada, M., Formentin, P., Iñiguez, B., Ferré-Borrull, J., Pallarés, J., Nolasco, J.C., Palomares, E., Sánchez, A., Marsal, L.F.: Performance and degradation of organic solar cells with different p. 3ht: pcbm[70] blend composition. In: Proceedings of the 8th Spanish Conference on Electron Devices, CDE 2011, pp. 1–4, February 2011
12. Yang, J.-F., Lu, C.-L.: Combined techniques of singular value decomposition and vector quantization for image coding. *IEEE Trans. Image Process.* **4**(8), 1141–1146 (1995)
13. Haralick, R.M., Shanmugam, K., Dinstein, I.: Textural features for image classification. *IEEE Trans. Syst. Man Cybern.* **SMC-3**(6), 610–621 (1973)
14. Capizzi, G., Sciuto, G.L., Napoli, C., Tramontana, E., Woźniak, M.: Automatic classification of fruit defects based on co-occurrence matrix and neural networks. In: 2015 Federated Conference on Computer Science and Information Systems (FedCSIS), pp. 861–867, September 2015
15. Klema, V., Laub, A.: The singular value decomposition: its computation and some applications. *IEEE Trans. Autom. Control* **25**(2), 164–176 (1980)
16. Lange, K.: *Singular Value Decomposition*, pp. 129–142. Springer, New York (2010)
17. Mak, M.W., Kung, S.Y.: Estimation of elliptical basis function parameters by the em algorithms with application to speaker verification. *IEEE Trans. Neural Networks* **11**(4), 961–969 (2000)